J Fluoresc (2011) 21:327–338
DOI 10.1007/s10895-010-0720-3

ORIGINAL PAPER

Molecular Geometry Optimization, Two-Photon Absorption and Electrochemistry of New Diphenylethylene Derivatives Linking with Benzophenone Moiety Through Ether Covalent Bond

Hongru Li · Fang Gao · Chunfeng Wang · Jianchao Wang · Shengtao Zhang

Received: 30 April 2010 / Accepted: 8 September 2010 / Published online: 13 October 2010

Abstract This paper presents the molecular geometry optimization, two-photon absorption and electrochemistry of new dyes containing benzophenone part, including 4-(*p*-benzoyl-benzyloxy)yl-4′-nitro-diphenylethylene (**C1**), 4-[N-methyl-N-(2-(*p*-benzoyl-benzyloxy)yl-ethyl]-4′-nitro-diphenylethylene (**C2**), 4-[N-ethyl-N-(2-(*p*-benzoyl-benzyloxy)yl-ethyl]-4′-nitro-diphenylethylene (**C3**), and 4-N, N-bis[(2-(*p*-benzoyl-benzyloxy)yl-ethyl]-4′-nitro-diphenyl ethylene (**C4**). The molecular structural parameters show that the coplanarity of diphenylethylene moiety is diminished in the excited state for **C1,** while it is enhanced for **C2**, **C3** and **C4**. The electron density distribution of frontier orbital suggests that the derivatives exhibit (π, π) transition with internal charge transfer character, and the extent of charge transfer of **C2, C3** and **C4** is larger than that of **C1**. The derivatives display remarkable two-photon absorption (TPA) induced up-converted emission under 800 nm Ti: Sapphire femtosecond laser excitation. The maximal TPA emission wavelength of **C2, C3** and **C4** is red-shifted with respect to that of **C1**. TPA cross sections of **C2**, **C3** and **C4** are larger than those of **C1**. The cyclic voltammograms and the fluorescence lifetimes of the derivatives were determined and discussed.

H. Li (✉) · F. Gao (✉) · C. Wang · J. Wang · S. Zhang
College of Chemistry and Chemical Engineering,
Chongqing University,
Chongqing, China 400044
e-mail: hongruli1972@gmail.com

F. Gao
e-mail: fanggao1971@gmail.com

Keywords Two-photon absorption · Molecular geometry optimization · Electrochemistry · Chromophore

Introduction

Two-photon polymerization receives considerable attention due to its wide applications such as data storage [1], microfabrication [2], hydrogel microstructure [3], protein microstructure [4] and DNA loading [5]. Marder considers that the achievement of 100 nm resolution of two-photon microfabrication is one of greatest targets in non-linear optical materials in the future decades [6]. This inspires the scientists to search for various strategies to obtain highly efficient two-photon polymerization. Marder and coauthors obtained highly efficient two-photon polymerization with various conjugative derivatives [7], which was explored by a number of other scientists [8–10]. On the other hand, unclear two-photon initiating mechanism of these derivatives makes it very hard to develop similar more efficient two-photon photoinitiators.

Since commercial ultraviolet photoinitators can be used for ultraviolet photocuring, Belfield and coworkers proposed that these photoinitators could be directly employed as two-photon photoinitators [11]. However, the short absorption wavelength and the small TPA cross section limit their application potentials in two-photon polymerization. To overcome these shortcomings, excellent TPA dyes were used to sensitize ultraviolet photoinitators under near-IR laser to achieve high efficient two-photon polymerization [12, 13], in which intermolecular TPA-induced dye-sensitization plays central role for the yields of free radicals.

While, it is not easy to increase further two-photon polymerization with this approach because intermolecular dye-sensitization photoreaction rate is always slower than intramolecular photoinduced dye-sensitization rate, and intermolecular dye-sensitization is affected by a number of factors, such as viscosity and polarity of the medium.

Hence, we assume that it is possible to achieve high efficiency two-photon polymerization through more rapid intramolecular photoinduced dye-sensitization if a two-photon chromophore is linked covalently with ultraviolet light photoinitator. However, the design and synthesis of such TPA derivatives and the investigation of their photophysical and photochemical nature are big challenges for chemists. Recently, our group reported such chromophore-linked ultraviolet light photoinitators via ether bond [14], in which chromophore groups have similar chemical structures, while benzophenone group locates in different substituted position. Two-photon optical properties of the derivatives have shown a strong relationship with the substituted position of benzopheone moiety. This article explores the survey of two-photon absorption properties of similar derivatives which have different chromophore chemical structures, while similar substituted position of benzophenone group. Of particular interests in this paper concentrates on the revealing the effect of chemical structures on the two-photon absorption properties. In order to reveal deeply the relationship between the chemical structures and two-photon absorption properties of these new derivatives, we further performed molecular geometry optimization and the fluorescence lifetimes and the cyclic voltammograms.

Experimental

Reagents and Materials

Organic solvents were obtained from Chongqing Medical and Chemical Corporation. Other chemicals and reagents were purchased from Aldrich unless otherwise specified. **C1** to **C4** were synthesized in our laboratory [14, 15] (Fig. 1). The organic solvents were dried using standard laboratory techniques according to the published methods [16].

Molecular Geometry Optimization

The calculations were performed by means of the Gaussian 03 program package. The geometry optimization of the derivatives for the ground electronic state (S_0) was carried out with HF (Hartree-Fock) method and at DFT (density functional theory) level using the B3LYP both [17–19], while the CIS (single-excitation configuration interaction) was employed to optimize the geometries of the first singlet excited state (S_1) of the derivatives. The physical condition was supposed in vacuum.

Although the CIS produces basically reliable geometries and force-fields, it predicts too much high excitation energies (*ca*. 1 eV). To correct the errors and introduce the dynamic electron correlation, DFT and TDDFT (time-dependent density functional theory) were performed to predict energies at the HF and CIS optimized geometries for S_0 and S_1 state respectively, such as DFT//HF or TDDFT//CIS (denoted as *single-point calculation//optimization method*), the latter was used to analyze the fluorescence properties in the excited state. The TDDFT//HF and TDDFT//DFT were used for the calculation of absorption spectra. All calculations were carried out with 6-31G** basis set.

Instruments

The UV/visible absorption spectra (1×10^{-5} mol/L) were recorded with a Cintra spectrophotometer. One-photon fluorescence (OPF) spectra (1×10^{-5} mol/L) were checked with Shimadzu RF-531PC spectrofluorophotonmeter. Rodamin 6G in ethanol (Φ=0.94, 1×10^{-6}–1×10^{-5} mol/L [20]) was used as reference to determine the fluorescence

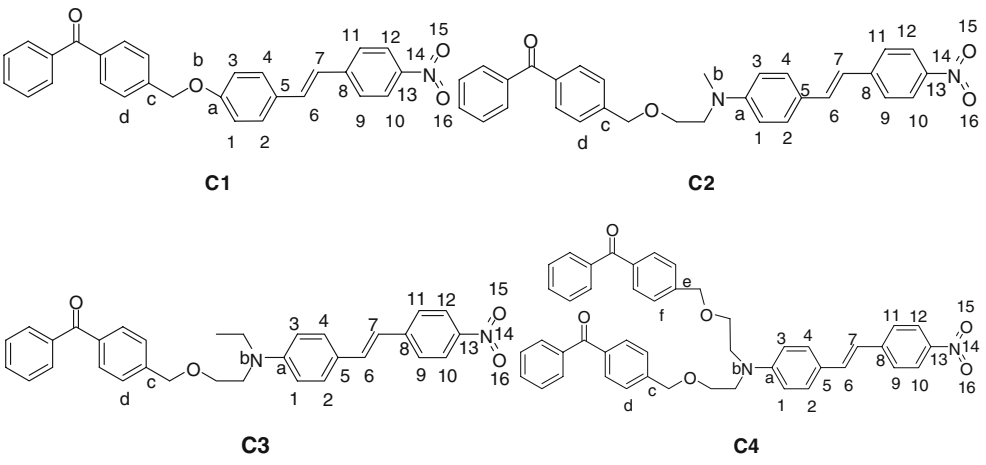

Fig. 1 Chemical structures of the derivatives with numbering some atoms

Table 1 Structural parameters of the ground state and the excited state of **C1** and **C2** (the data of **C2** is in the bracket)

Structural parameters	S_0 (*HF/6-31G***)	S_0' (*DFT/B3LYP/6-31G***)	S_1 (*CIS/6-31G***)
C(5)-C(6)	1.47431 (1.46569)	1.46055 (1.45484)	1.47534 (1.40561)
C(6)-C(7)	1.32832 (1.33515)	1.35090 (1.35347)	1.32788 (1.39952)
C(7)-C(8)	1.47536 (1.46913)	1.46110 (1.45849)	1.47578 (1.40605)
C(13)-N(14)	1.45445 (1.44114)	1.46047 (1.46144)	1.39921 (1.42055)
N(14)-O(15)	1.19458 (1.22821)	1.23279 (1.23368)	1.25616 (1.20567)
N(14)-O(16)	1.19458 (1.22817)	1.23270 (1.23359)	1.25612 (1.20524)
C(2)-C(5)-C(6)-C(7)	22.151 (−14.494)	−0.053 (0.420)	−23.602 (−0.671)
C(5)-C(6)-C(7)-C(8)	−179.679 (179.827)	−179.903 (−179.895)	179.310 (179.301)
C(6)-C(7)-C(8)-C(9)	−156.849 (158.351)	179.815 (179.945)	156.477 (179.641)
C(10)-C(13)-N(14)-O(16)	0.101 (−0.102)	−0.096 (−0.045)	−11.290 (0.009)
C(12)-C(13)-N(14)-O(15)	−0.471 (0.458)	−0.098 (−0.044)	12.808 (0.016)
C(2)-C(5)-C(13)-C(10)	41.410 (−32.885)	−0.050 (0.432)	−43.203 (−1.703)
C(d)-C(c)-C(2)-C(5)	−142.842 (59.347)	−144.363 (59.356)	−142.875 (59.402)

Bond distances and bond angles are given in Angstroms and Degree.

S_0 calculated with HF/6-31G**; S_0' calculated with DFT/B3LYP/6-31G**; S_1 calculated with CIS/6-31G**.

quantum yields of the compounds herein. To avoid self-quenching of fluorescence emission, the low concentration of the sample (1×10^{-6} mol/L) was prepared for the survey of fluorescence quantum yields. The fluorescence lifetimes were determined using an Edinburgh FLS920 time-resolved fluorescence spectrometer using a least-square method.

The two-photon fluorescence (TPF) spectra were determined with a streak camera (C5680-01, Hamamatsu) and imaging spectrography (C5094, Hamamatsu). The pump laser beam came from a mode-locked Ti:sapphire laser system operating at 800 nm, pulse duration <200 fs and repetition rate 76 MHz (Coherent Mira900-D). TPA cross sections of the derivatives were calculated by the following equations:

$$\sigma_2 = \frac{\sigma^{\mathrm{TPE}}}{\Phi_{\mathrm{F}}} \tag{1}$$

$$\sigma^{\mathrm{TPE}} = \sigma_{\mathrm{cal}}^{\mathrm{TPE}} \frac{c_{cal}}{c} \frac{n_{cal}}{n} \frac{S}{S_{cal}} \tag{2}$$

Wherein σ is two-photon absorption section, $\boldsymbol{\sigma^{TPE}}$ is two-photon excited crossing section, $\boldsymbol{c}$ is the concentration

Table 2 Structural parameters of the ground state and the excited state of **C3** and **C4** (the data of **C4** is in the bracket)

Structural parameters	S_0 (*HF/6-31G***)	S_0' (*DFT/B3LYP/6-31G***)	S_1 (*CIS/6-31G***)
C(5)-C(6)	1.47061(1.46971)	1.45586(1.45462)	1.40524(1.40517)
C(6)-C(7)	1.32947(1.32988)	1.35298(1.35356)	1.39976(1.39935)
C(7)-C(8)	1.47429(1.47386)	1.45896(1.45842)	1.40570(1.40606)
C(13)-N(14)	1.45369(1.45334)	1.46221(1.46137)	1.42199(1.42113)
N(14)-O(15)	1.19482(1.19493)	1.23343(1.23368)	1.20472(1.20552)
N(14)-O(16)	1.19477(1.19490)	1.23338(1.23363)	1.20516(1.20510)
C(2)-C(5)-C(6)-C(7)	15.182(−15.489)	−0.697(−2.367)	−0.578(−0.912)
C(5)-C(6)-C(7)-C(8)	−179.825(179.767)	179.900(179.793)	178.933(179.138)
C(6)-C(7)-C(8)-C(9)	−157.992(158.378)	−179.681(177.894)	179.690(179.462)
C(12)-C(13)-N(14)-O(15)	−0.461 (0.464)	0.064(−0.025)	0.014 (0.024)
C(10)-C(13)-N(14)-O(16)	0.112(−0.099)	0.054(−0.132)	0.011 (0.007)
C(2)-C(5)-C(13)-C(10)	33.757(-33.812)	−0.523(−4.047)	−2.016(−2.226)
C(d)-C(c)-C(2)-C(5)	62.322(76.079)	68.932(64.309)	63.703(69.757)
C(f)-C(e)-C(2)-C(5)	87.808	97.868	101.745

Bond distances and bond angles are given in Angstroms and Degree.

S_0 calculated with HF/6-31G**; S_0' calculated with DFT/B3LYP/6-31G**;S_1 calculated with CIS/6-31G**.

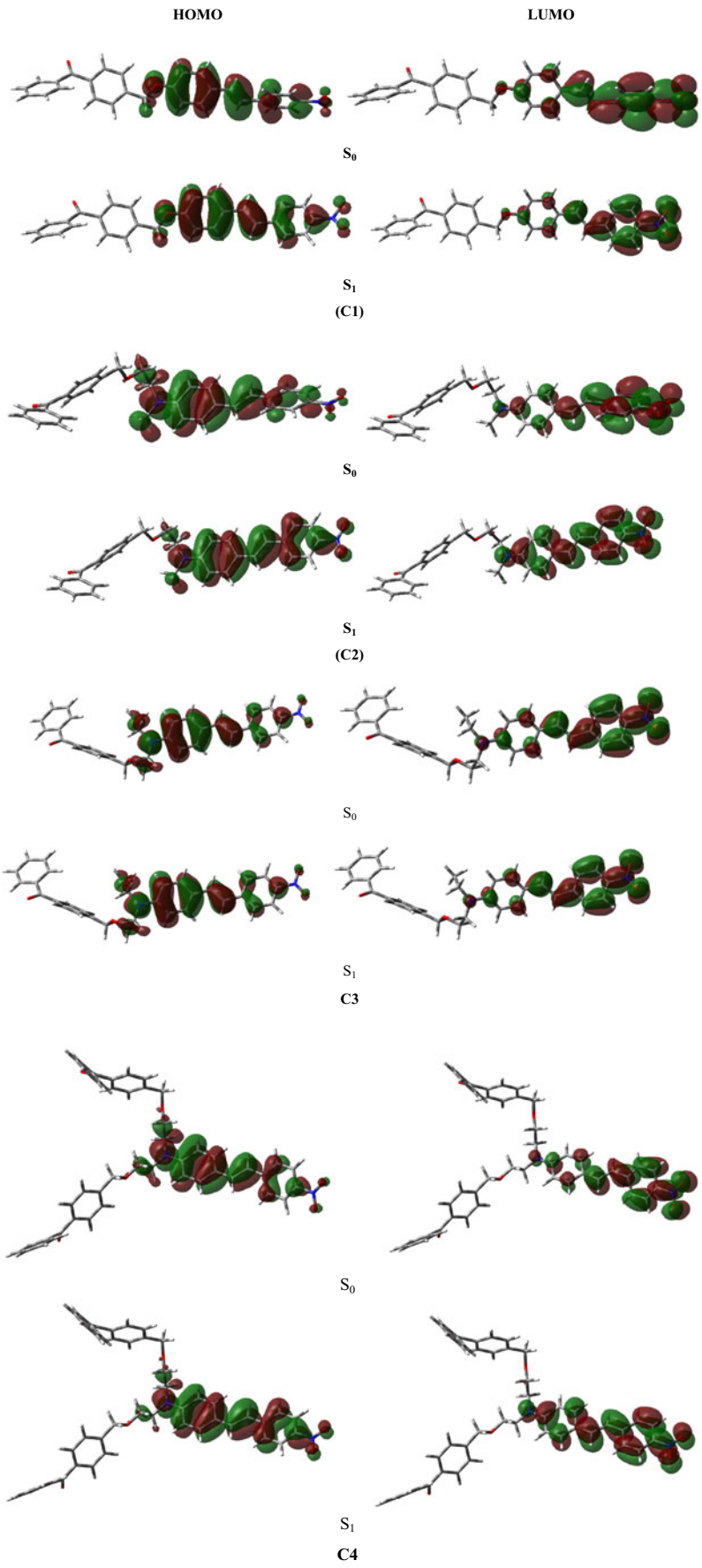

Fig. 2 Electron density distribution of frontier molecular orbital of the derivatives in S_0 and S_1

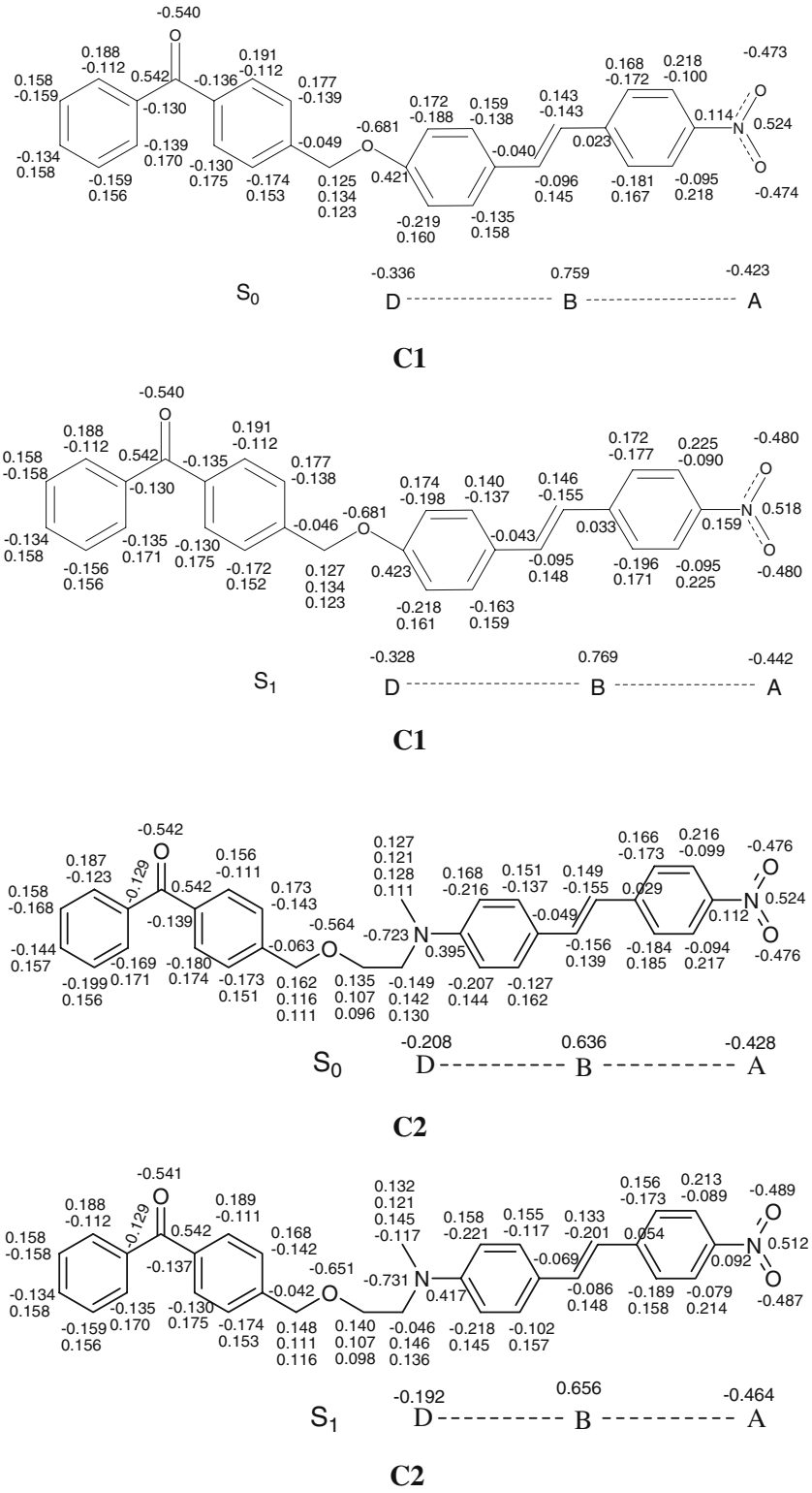

Fig. 3 Mulliken charge distribution of S_0 and $S_1$of **C1**, **C2, C3** and **C4**

of reference and sample molecules, ***n*** is the refractive index of the solvent, and ***S*** is TPA fluorescence intensity, ***cal*** is denoted as reference. Herein, rodamin-6G was employed as reference, which has TPA cross section as 35 GM in methanol (5×10^{-4} mol/L [21]). The sample solution was removed oxygen through bubbling nitrogen gas for fifteen minutes before the measurement of one-photon and two-photon induced emission.

Fig. 3 (continued)

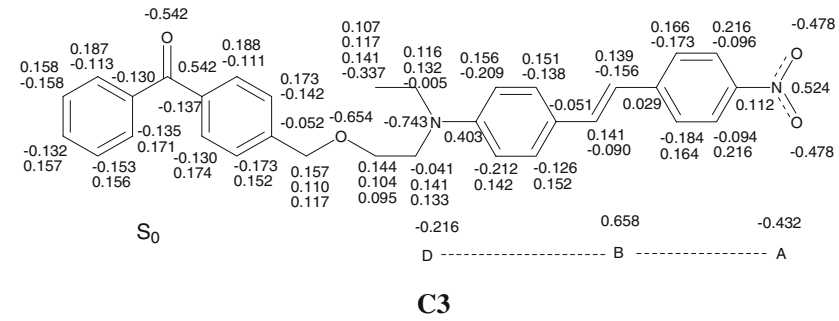

C3

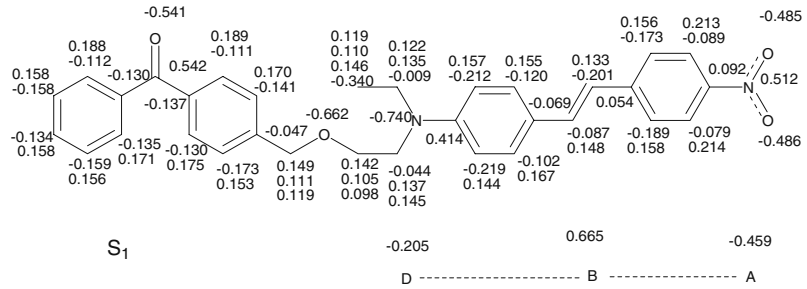

C3

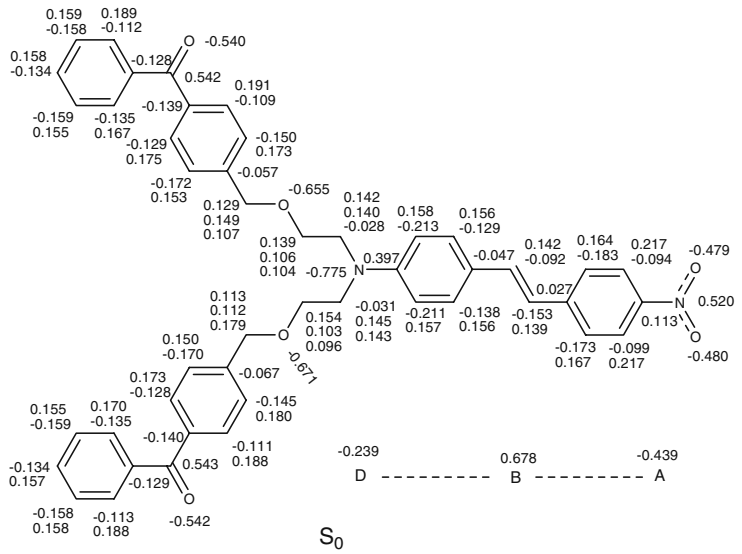

C4

Electrochemical Measurement

The cyclic voltammograms were carried out with a Shanghai Chenhua working station. Two Pt work electrodes and an Ag/Ag^{+} reference electrode were included in a cell. Typically, a 0.05 mol/L solution of tetra-n-butylammonium hexaflorophosphate in methylene chloride (CH_2Cl_2) containing of the derivatives was bubbled with argon for 15 min before the measurement.

Results and Discussion

Structural Parameters

Tables 1 and 2 presents the geometric parameters of the derivatives in the ground state (S_0) and excited singlet state (S_1). Tables 1 and 2 shows that the dihedral angel of α[C(2)-C(5)-C(6)-C(7)] of the all derivatives obtained with HF level is much larger than that obtained by DFT

Fig. 3 (continued)

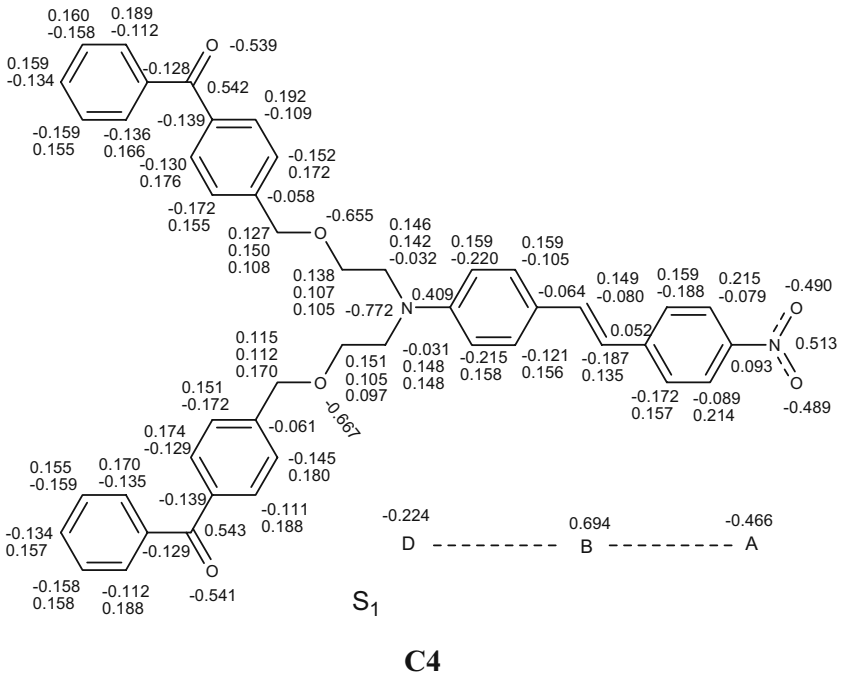

level. For example, the dihedral angel α of **C1** with HF level is 22.151°, while the dihedral angel α of **C1** with DFT level is −0.053°. This suggests the planarity of the derivatives obtained by DFT level is better than that calculated by HF level. While according to Brillouin theory [22], CIS method of the excited state is equivalent to HF method in the ground state, hence, the results from CIS and HF are compared particularly herein. For all derivatives, the bond lengths between C_5, C_6, C_7, C_8 tend to be even as excited from S_0 to S_1. The data (Tables 1 and 2) show that θ[C(2)-C(5)-C(13)-C(10)] of the derivatives has some torsion in the opposite directions, which means that diphenylethylene unit in these derivatives are not coplanar in S_0. In S_1 of **C1**, diphenylethylene part show larger torsion in the opposite direction. The dihedral angle θ of **C1** is changed from 41.410° in S_0 to −43.203° in S_1, and thus its conjugative nature is reduced further in S_1. While as sharp contrast, diphenylethylene units in **C2**, **C3** and **C4** tend to be coplanarity in S_1. For example, the dihedral angle θ of **C2** is reduced from −32.885° in S_0 to −1.703° in S_1, and thus the conjugative nature is enhanced. The dihedral angels of C(10)-C(13)-N(14)-O(16) and C(12)-C(13)-N(14)-O(15) of the derivatives indicate that nitro and its adjacent phenyl ring are almost located the same plane in the ground state, and they show small changes from S_0 to S_1. In a word, the changes of molecular geometry occur mainly in diphenylethylene part as excited from S_0 to S_1 for these derivatives.

Frontier Orbitals, Energy, Dipolar Moment Changes and Mulliken Charges

Figure 2 shows the electronic density distribution in HOMO and LUMO orbitals in S_0 and S_1. A symmetrical π-type orbital is observed in HOMO and LUMO, which indicates that the derivatives could proceed (π, π) transition with internal charge transfer nature [23]. As presented in Fig. 2, the electronic density is located mainly at diphenylethylene part in HOMO for the derivatives in S_0 and S_1. While, the electronic density is distributed mainly at nitro group and its adjacent phenyl ring in LUMO for the derivatives in S_0 and S_1, and the electronic density distribution is closer to nitro group for **C2**, **C3** and **C4** because the amino groups have stronger electron donating effect. We calculated further the

Table 3 The theoretical energies and energy gaps of HOMO and LUMO of the derivatives in S_0 and S_1

States		Energy (eV)			
		C1	C2	C3	C4
S_0	HOMO	−5.8995	−5.2004	−5.2072	−5.3786
	LUMO	−2.4774	−2.2632	−2.2694	−2.3377
	Gaps	3.4221	2.9372	2.9378	3.0409
S_1	HOMO	−6.0246	−4.9941	−5.0597	−5.1958
	LUMO	−2.7252	−2.2411	−2.4259	−2.5130
	Gaps	3.2994	2.7530	2.6338	2.6828

Table 4 Calculated the absorption and fluorescence wavelength (nm) and vibration strength (*f*) of the derivatives

Compounds			λ/nm	*f*	E/ev	Compositions
C1	UV	1	369.6	0.8120	3.35	H-0→L+0(+89%)
		2	333.9	0.0011	3.71	H-1→L+1(+74%)
		3	322.8	0.0003	3.84	H-0→L+1(+98%)
	Fluo	1	586.3	0.0002	2.11	H-1→L+(+84%)
		2	406.4	0.6987	3.05	H-0→L+0(+88%)
		3	333.9	0.0014	3.71	H-2→L+1(+75%)
C2	UV	1	427.0	0.6902	2.90	H-0→L+0(+89%)
		2	377.8	0.0000	3.28	H-0→L+1(+100%)
		3	333.2	0.0013	3.72	H-2→L+1(+38%)
	Fluo	1	451.8	1.3611	2.74	H-0→L+0(+75%)
		2	411.5	0.0001	3.01	H-0→L+1(+100%)
		3	332.7	0.0017	3.73	H-2→L+1(+74%)
C3	UV	1	417.4	0.7493	2.97	H-0→L+0(+90%)
		2	375.5	0.0002	3.30	H-0→L+1(+100%)
		3	352.4	0.0001	3.52	H-0→L+2(+100%)
	Fluo	1	453.4	1.3927	2.73	H-0→L+0(+75%)
		2	411.2	0.0001	3.01	H-0→L+1(+100%)
		3	325.8	0.2273	3.81	H-0→L+2(+68%)
C4	UV	1	430.5	0.7110	2.88	H-0→L+0(+89%)
		2	382.2	0.0000	3.24	H-0→L+1(+100%)
		3	332.8	0.0013	3.73	H-2→L+1(+72%)
	Fluo	1	448.1	1.4420	2.77	H-0→L+0(+75%)
		2	408.6	0.0002	3.03	H-0→L+1(+100%)
		3	381.3	0.0001	3.25	H-0→L+2(+100%)

UV the maximal ultraviolet/visible absorption, nm; *Fluro* the maximal fluorescence emission, nm

net charges of electron-donating unit (D), bridging unit (B) and electro-accepting unit (A) of the derivatives in S_0 and S_1, and the results are shown in Fig. 3. Remarkably, the data demonstrate that the derivatives do exhibit internal charge transfer, in which **C2**, **C3** and **C4** display larger extent of internal charge transfer due to stronger electron-donating effect of amino group. Hence, the dipole moment changes between the excited state and ground state of **C2**, **C3** and **C4** are higher than that of **C1** (1.46 D in **C1**, 2.90 D in **C2**, 2.53 Debye in **C3**, 2.32 D in **C4**). We also calculated H-L energy levels for the derivatives, and the results in Table 3 show that HOMO and LUMO energy levels of **C1** are lower than those of **C2**, **C3** and **C4**, while H-L gaps of **C1** in S_0 and S_1 are higher than those of the other derivatives.

Table 4 confirms further that (π, π^*) electron transition from H-0→L+0 takes places efficiently, and the maximal oscillator strengths (*f*) are 0.8120, 0.6902, 0.7493, 0.7110 with corresponding transition probabilities 89%, 89%, 90%, 89% for **C1** to **C4**. Accordingly, the derivatives emit through L+0→H-0 electron transition, which have the maximal *f* values 0.6987, 1.3611, 1.3927, 1.4420 with corresponding transition probabilities 88%, 75%, 75%, 75% respectively. The calculated absorption and emission spectroscopy in Fig. 4 shows that the derivatives **C2**, **C3** and **C4** exhibit remarkable red-shift, which is nice agreement with the experimental results. The differences on the electron density distribution in HOMO and LUMO, the dipole moment changes between S_0 and S_1, and H-L energy gaps could be the basic factors causing the red-shift of absorption and emission wavelength for **C2** to **C4**. We would point out that theoretical maximal emission wavelength of the derivatives is not so accordance with experimental survey (see Tables 3 and 4, for instances the maximal OPF emission of **C2** in THF 609 nm), which could be mostly due to extremely low polarity of vacuum [24].

TPA Emission and TPA Cross Section

Because **C1** has strong emission in CH_2Cl_2, while **C2**, **C3** and **C4** exhibit remarkable emission in benzene, we determined TPA emission of **C1** in tetrahedronfuran (THF) and CH_2Cl_2, and measured TPA emission of **C2**, **C3** and **C4** in benzene and THF. Figure 5 presents TPA emission of the derivatives under 800 nm Ti:squassier laser in THF. The maximal TPA emission wavelength of **C2**, **C3** and **C4** is much red-shifted with respect to that of **C1**

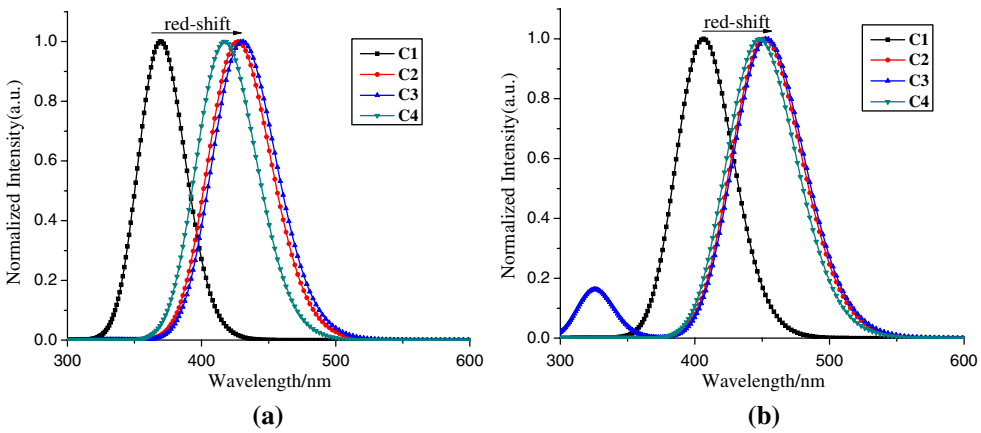

Fig. 4 Normalized calculated absorption spectra (**a**) and fluorescence spectra (**b**) of the derivatives

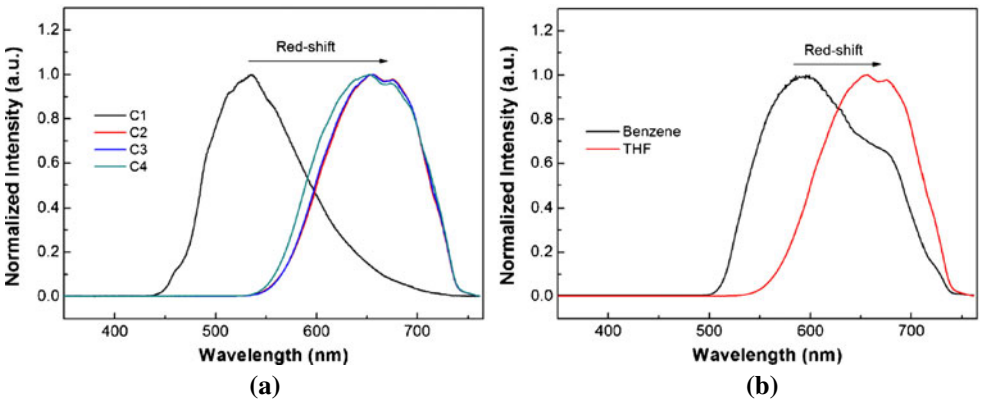

Fig. 5 Normalized TPA emission of the derivatives excited by 800 nm Ti: sapphire laser (a) in THF; (b) **C2** in benzene and THF

(Fig. 5 (a)). The maximal TPA emission wavelength of **C2** exhibits red-shift with the increasing polarity of the solvents, as shown in Fig. 5 (b). Two-photon optical parameters of the derivatives are presented in Table 5. The data show that: (1) The maximal TPA emission wavelength is red-shifted with the increasing polarity of the solvents for the same derivative. (*ca. 40–50 nm*) (2) In the same solvent, the maximal TPA emission wavelength of **C2, C3** and **C4** exhibits red-shift with respect to that of **C1**. (*ca. 100 nm*) (3) In the same solvent, **C2**, **C3** and **C4** have larger TPA cross sections than **C1**, and **C4** has the largest TPA cross sections (*421.3GM in THF*). (4) For the same derivative, the TPA cross section of the derivatives is larger in polar solvents. (5) Two-photon optical parameters of **C2**, **C3** and **C4** in benzene are similar to those of **C1** in CH_2Cl_2.

As discussed, **C2**, **C3** and **C4** exhibit much larger extent of internal charge transfer, and thus they have a larger dipole moment changes between the ground state and the excited state. Furthermore, the derivatives **2**, **3** and **4** show better conjugative properties in the excited state. These could cause not only the red-shift of the maxima TPA mission wavelength for the derivatives **2**, **3** and **4**, but larger TPA cross sections [25, 26]. The results also show that **C4** displays branch effect. Furthermore, the results indicate that even if in polar CH_2Cl_2, the extent of the intramolecular charge transfer of **C1** could be smaller than that of **C2**, **C3**

Table 5 Two-photon spectral data of the derivatives in various solvents

Compounds	Optical parameters	Solvents		
		Benzene	THF	CH_2Cl_2
C1	λ_{max} (OPA), (nm)	360	370	375
	λ_{max} (OPF), (nm)		507	541
	Φ	tiny	0.034	0.20
	λ_{max} (TPF), (nm)		535	585
	σ (GM)		24.1	102.3
C2	λ_{max} (OPA), (nm)	435	440	440
	λ_{max} (OPF), (nm)	550	609	
	Φ	0.36	0.054	tiny
	λ_{max} (TPF), (nm)	595	655	
	σ (GM)	110.8	344.3	
C3	λ_{max} (OPA), (nm) [15]	436	442	441
	λ_{max} (OPF), (nm) [15]	551	607	
	Φ [15]	0.36	0.053	tiny
	λ_{max} (TPF), (nm)	595	656	
	σ (GM)	113.5	407.6	
C4	λ_{max} (OPA), (nm) [15]	431	436	439
	λ_{max} (OPF), (nm) [15]	556	608	
	Φ [15]	0.47	0.063	tiny
	λ_{max} (TPF), (nm)	589	652	
	σ (GM)	104.5	421.3	

OPA one-photon absorption, *OPF* one-photon fluorescence, *TPF* two-photon fluorescence, σ: two-photon cross- section (GM, 1GM= 10^{-50} cm·s·photo^{-1})

Table 6 The fluorescence lifetimes and the transition constants of $S_1$of the derivatives in various solvents

Solvents	C1			C2			C3			C4		
	τ	K_r	K_{nr}	τ	K_r	K_{nr}	τ	K_r	K_{nr}	τ	K_r	K_{nr}
Benzene				2.69	1.34	2.38	2.82	1.26	2.29	2.68	1.76	1.97
CH_2Cl_2	2.63	0.76	3.04									

τ ns, K_r, K_{nr}: 10^8 /s

and **C4** in benzene. The results demonstrate that two-photon optical nature is shown to be related closely to chemical structures of chromophore part.

Table 5 also shows that TPA emission wavelnegth of the derivatives is red-shifted with respect to one-photon emission wavelength in the same solvent (*ca. 30–40 nm*), which could be ascribed to reabsorption effect [27–33]. In fact, various TPA compounds exhibit such red-shift phenomenon (*from 30–70 nm*) [27–33]. The existence of overlap of the absorption and emission spectra of the derivatives makes it possible that part of the emission is reabsorbed by the solution. One-photon excitation beam has much shorter length than that of two-photon excitation beam due to strong linear absorption of one-photon excitation beam. Consequently, one-photon fluorescence emits from the surface of the sample and reabsorption effect could be ignored. Since 800 nm laser could penetrate deeply in the solution, and TPA measurement was performed in the concentrated sample solution, as a result, the reabsorption effect of TPA fluorescence becomes remarkably larger than that of one photon emission.

Fluorescence Lifetimes

The fluorescence lifetimes of the derivatives **1** to **4** were determined to understand further the excited state properties of the derivatives, and the results were listed in Table 6. The fluorescence lifetime of **C1** in CH_2Cl_2 is close to those of the derivatives **2** to **4** in benzene. Remarkably, TPA optical parameters of **C1** in CH_2Cl_2 is also close to those of **C2** to **C4** in benzene. This indicates that such photophysical results could be caused by the same factor. We shall point out that the fluorescence lifetimes of derivatives **1** to **4** are much longer than that of simple stilbene (τ, 0.075 ns) [34], even larger than that of stilbenoid dendrimers bearing with dibutylamino groups (2.1–2.2 ns) [35]. It was well demonstrated that for a simple stilbene, "cis-trans" isomerization is the main approach of deacativation of S_1 [36]. In the present study, intramolecular charge transfer and twisted intramolecular charge transfer states could dominate the deacativation of S_1 rather than "cis-trans" isomerization due to the "D-π-A" molecular character of the derivatives, and the fluorescence lifetimes of stilbene derivatives is thus enlarged. The radiation transition constants (K_r) and non-radiation transition constants (K_{nr}) of the derivatives were calculated according to the following equations:

$$Kr = \frac{\Phi_F}{\tau}, \tag{3}$$

$$Knr = \frac{1 - \Phi_F}{\tau} \tag{4}$$

wherein Φ_F is fluorescence quantum yield, τ represents as fluorescence lifetime, K_r is radiation transition constant, K_{nr} is non-radiation transition constant. Table 6 shows that **C2, C3** and **C4** exhibit more efficient radiation transition at the excited singlet state than **C1**. This suggests that the excited singlet state is correlated to the intramolecular charge transfer of the derivatives.

Cyclic Voltammograms

Figure 6 presents the cyclic voltammetric curves of derivatives **3** and **4** in CH_2Cl_2. **C3** and **C4** exhibit irreversible redox processes under all sweeping rates from

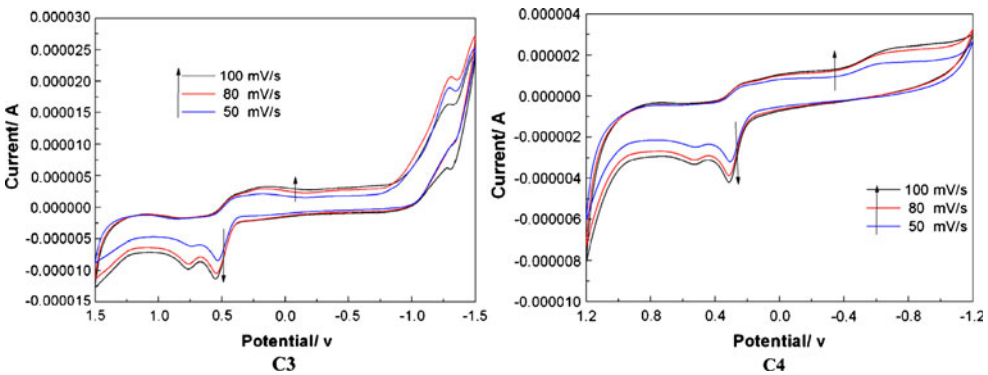

Fig. 6 Cyclic voltammetries of **1** to **4** in methylene chloride at various scan rates

Table 7 Estimated HOMO and LUMO energies of the derivatives from cyclic voltammograms

Derivatives	E^{OX}/V	λ_{onset}/nm	E_g/eV	E_{HOMO}/eV	E_{LUMO}/eV
C1	1.21	436	2.84	−8.39	−5.55
C2	0.63	516	2.40	−7.37	−4.97
C3	0.76	525	2.36	−7.46	−5.10
C4	0.52	520	2.38	−7.24	−4.86

$E_{LUMO} = -E^{OX} - 4.34$[40, 41], $E_{gap} = 1240/\lambda_{onset}$, $E_{LUMO} = E_{HOMO} + E_g$

50 to 100 mV·s^{-1}, which is similar to those of **C1** and **C2** [37]. Furthermore, the linear increasing of peak currents with the square root of scan rates suggests that the redox processes of the derivatives are well dominated by the diffusion-controlled electron transfer reactions [38]. It is interesting that **C1** has a larger oxidation potential (1.210 V) than those of **C2** (0.63, 0.40 V), **C3** (0.76, 0.55 V) and **C4** (0.52, 0.31 V). This could be ascribed to strong electron-donating effect of amino groups, which could lower oxidative potentials [39].

HOMO-LUMO energy levels of the derivatives were estimated further from redox potentials and the optical band gap (E_g), which was calculated from the onset of the longest absorption wavelength at 10% of the maximal UV peak. The estimated data are presented in Table 7. The results show clearly that the energy levels of HOMO and LUMO of **C1** are lower than those of **C2**, **C3** and **C4**, while its HOMO-LUMO gap is larger that those of the derivatives **2**, **3** and **4**, which is prefect consistent with calculated results. This demonstartes that both HOMO and LUMO energies and HOMO-LUMO gaps of the derivatives exhibit remarkable dependence on the chemical structures of chromophore groups.

Conclusions

Molecular geometry optimization of the derivatives containing benzophenone moiety via covalent ether bond shows that structural parameters, electron density distribution in frontier orbital, internal charge transfer, dipole moment changes between the excited state and ground state, energy levels and energy gaps of frontier orbital have a close interrelationship with chromophore parts, which is further confirmed by electrochemical survey of the derivatives. These could be the fundamental reasons that one and two photon optical properties of the derivatives are related to the chromophore parts. The results suggest that it is possible to tune the nature of the excited state of such derivatives containing benzophenone part by the variation of chromophore parts, and thus TPA nature of such derivatives could be tuned.

Acknowledgements The authors appreciate financial support from National Natural Science Foundation of China (Nos. 20776165, 20702065, 20872184). We would thank "the Foundation of Chongqing Science and Technology Commission" (CSTC2008BA4020, CSTC2009BB4216). We also thank the support from the Key Laboratory of Functional Crystals and Laser Technology, TIPC, Chinese Academy of Sciences, and the support from "Innovative Talent Training Project, the Third State of "211 Project, S-09103", Chongqing University.

References

1. Belfield KD, Schafer KJ (2002) A new photosensitive polymeric material for WORM optical data storage using multichannel two-photon fluoreescence readout. Chem Mater 14(9):3656–3662
2. Lee KS, Kim RH, Yang DY, Park SH (2008) Advances in 3D nano/microfabrication using two-photon initiated polymerization. Prog Polym Sci 33(6):631–681
3. Watanabe T, Akiyama M, Totani K, Kuebler SM, Stellacci F, Wenseleers W, Braun K, Marder SR, Perry JW (2002) Photo-responsive hydrogel microstructure fabricated by two-photon initiated polymerization. Adv Funct Mater 12(611):614
4. Pitts JD, Howell AR, Taboada R, Banerjee I, Wang J, Goodman SL, Campagnola PP (2002) New photoactivators for multiphoton excited three-dimensional cross-linking of proteins: bovine serum albumin and type 1 collagen. Photochem Photobiol 76(2):135–144
5. Gupta P, Markowicz PP, Baba K, O'Reilly J, Samoc M, Prasad PN (2006) DNA-ormocer based biocomposite for fabrication of photonic structures. Appl Phys Lett 88:213109-1–213109-3
6. Belfield KD, Ren XB, Van EWV, Hagan DJ, Dubikovsky V, Miesak EJ (2000) Near-IR two-photon photoinitiated polymerization using a fluorone/amine initiating syetem. J Am Chem Soc 122(6):1217–1218
7. Cumpston BH, Anathavel SP, Barlow S, Dyer DL, Ehrlich JE, Erskine LL, Heikal AA, Kuebler SM, Lee IYS, McCord-Maughon D, Qin J, Rockel H, Rumi M, Wu XL, Marder SR, Perry JW (1999) Two-photon polymerization initiators for 3D optical data storage and microfabrication. Nature 398(51):54
8. Zhou WH, Kuebler SM, Braun KL, Yu T, Cammack JK, Ober CK, Perry JW, Marder SR (2002) An efficient two-photon-generated photoacid applied to positive-tone 3D microfabrication. Science 296:1106–1109
9. Zhou WH, Kuebler SM, Perry JW, Marder SM (2002) Efficient photoacids based upon triarylamine dialkylsulfonium salts. J Am Chem Soc 124:1897–901
10. Kuebler SM, Braun KL, Zhou WH, Cammack JK, Yu T, Ober CK, Marder SR, Perry JW (2003) Design and application of high-sensitivity two-photon initiators for three-dimensional micro-fabrication. J Photochem Photobiol A Chem 158:163–170
11. Schafer J, Hales J, Balu M, Belfield K, Van Steryland E, Hagan D (2004) Two-photon absorption cross-sections of common photo-initiators J. Photochem Photobio A Chem 162:497–502
12. Li C, Luo L, Wang S, Huang W, Gong Q, Yang YY, Feng SJ (2001) Two-photon microstructure-polymerization initiated by a coumarin derivative/iodonium salt system. Chem Phys Lett 340:444–448
13. Wu J, Zhao Y, Li X, Shi M, Wu F, Fang X (2006) Multibranched benzylidene cyclopentanone dyes with large two-photon absorption cross-sections. New J Chem 30:1098–1103
14. Gao F, Hu ND, Wang JC, Yang LF, Yang L, Li HR, Zhang ST (2008) Synthesis, two-photon properties and electrochemistry of A-B2 type nitro-stilbene dyes with benzophenone groups. Acta Phys -Chem Sin 25(7):1320–1326

15. Gao F, Liu J, Peng HY, Hu ND, Li HR, Zhang ST (2010) Synthesis, spectroscopy and photochemistry of novel branched fluorescent nitro-stilbene derivatives with benzopheonone groups. J Fluorescence 20:703–712
16. Perrin DD, Armarego WLF, Perrin DR (1966) Purification of laboratory chemicals. Pergamon, New York
17. Scalmani G, Frisch MJ (2006) Geometries and properties of excited states in the gas phase and in solution: theory and application of a time-dependent density functional theory polarizable continuum model. J Chem Phys 124:094107-1–094107-12
18. Yi P, Liang YH, Cao C (2005) Intramolecular proton or hydrogen-atom transfer in the ground- and excited-states of 2-hydroxybenzophenone: a theoretical study. Chem Phys 315:297–302
19. Liang YH, Yi PG (2007) Theoretical studies on structure, energetic and intramolecular proton transfer of alkannin. Chem Phys Lett 438:173–177
20. Fischer M, Georges J (1996) Fluorescence quantum yield of rhodamine 6G in ethanol as a function of concentration using thermal lens spectrometry. Chem Phys Lett 260:115–118
21. Xu C, Webb WW (1996) Measurement of two-photon excitation cross sections of molecular fluorophores with data from 690 to 1050 nm. J Opt Soc Am B 13:481–491
22. Brillouin L (1943) Theory of the MagnetronIII. Phys Rev 63:127–131
23. Wang S, Kim SH (2009) Photophysical and electrochemical properties of D–π–A type solvatofluorchromic isophorone dye for pH molecular switch. Current Appl Phys 9:783–787
24. Singh AK, Ramakrishna G, Ghosh HN, Palit DK (2004) Photophysics and ultrafast relaxation dynamics of the excited states of dimethylaminobenzophenone. J Phys Chem A 108:2583–2597
25. Zhang XB, Feng JK, Ren AM (2007) Theoretical study of one- and two-photon absorption properties of octupolar D_{2d} and D_{3d} bipyridyl metal complexes. J Phys Chem A 111(7):1328–1338
26. Zhang XB, Feng JK, Ren AM, Sun CC (2006) Theoretical study of one- and two-photon absorption properties of olenfin-linked paracyclophane oligomers. Can J Chem 84(9):1114–1123
27. Tian L, Hu Z, Shi P, Zhou H, Wu J, Tian Y, Zhou Y, Tao X, Jiang M (2007) Synthesis and two-photon optical characterization of D–π–D type Schiff bases. J Lumin 127:423–430
28. Fitlis I, Fakis M, Polyzos I, Giannetas V, Persephonis P, Vellis P, Mikroyannidis J (2007) A two-photon absorption study of fluorene and carbazole derivatives. The role of the central core and the solvent polarity. Chem Phys Lett 447:300–304
29. Yan Y, Fan H, Guo Y, Lam C, Huang H, Sun Y, Tian L, Wang C, Tian Y, Wang H, Chen X (2007) Synthesis and two-photon absorption property of new π-conjugated dendritic fluorophores containing styrylpyridyl moieties. Mater Chem Phys 101:329–335
30. Wu L, Tang X, Jiang M, Tung C (1999) Two-photon induced fluorescence of novel dyes. Chem Phys Lett 315:379–382
31. Meng F, Mi J, Qian S, Chen K, Tian H (2003) Novel linear and tri-branched copolymers based on triphenylamine for non-doping emitting materials. Eur Polym J 39:1325–1331
32. Hua L, Li B, Meng F, Ding F, Qian S, Tian H (2004) Two-photon absorption properties of hyperbranched conjugated polymers with triphenylamine as the core. Polymer 45:7143–7149
33. Xing J, Chen W, Dong X, Tanaka T, Fang X, Duan X, Takata S (2007) Synthesis, optical and initiating properties of new two-photon polymerization initiators: 2, 7-Bis(styryl)anthraquinone derivatives. J Photochem Photobiol A: Chem 189:398–404
34. Uda M, Mizutani T, Hayakawa J, Momotake A, Ikegami M, Nagahata R, Arai T (2002) Photoisomerization of stilbene dendrimers: the need for a volume-conserving isomerization mechanism. Photochem Photobio 76:596–605
35. Segura JL, Gomez R, Martin N, Guldi DM (2001) Synthesis of photo- and electroactive stilbenoid dendrimers carrying dibutylamino peripheral groups. Org Lett 3:2645–2648
36. Squella JA, Sturm JC, Weiss-Lopez B, Bonta M, Nunez-Vergara LJJ (1999) Electrochemical study of β-nitrostyrene derivatives: steric and electronic effects on their electroreduction. J Electroana Chem 466:90–98
37. Gao F, Peng H, Yang L, Liu X, Wang J, Hu N, Xie T, Li H, Zhang S (2009) Visible light photopolymerization of nitro-stilbenzene photosensitive initiating systems. Poly Adv Tech 20(12):1010–1016
38. Aoki K, Guo Y, Chen JY (2009) Diffusion-controlled currents in viscous solutions of polyethylene glycols. J Electroanal Chem 629 (1–2):73–77
39. De S, Girigoswami A, Mandal S (2002) Enhanced fluorescence of triphenylmethane dyes in aqueous surfactant solutions at supramicellar concentrations-effect of added electrolyte. Spectrochimica Acta Part A 58:2547–2555
40. Liu J, Tu G, Zhou Q, Cheng Y, Geng Y, Wang L, Ma D, Jing X, Wang F (2006) Highly efficient green light emitting polyfluorene incorporated with 4-diphenylamino-1, 8-naphthalimide as green dopant. J Mater Chem 16:1431–1438
41. Bard AJ, Faulkner L (1984) Electrochemical methods-fundamentals and applications. Wiley, New York